Chapter 5

Crystallochemistry of clay minerals, weathering processes and evolution of continental surfaces

Balan E., Allard T., Morin G., Fritsch E., Calas G.

Institute of Mineralogy and Physics of Condensed Media (IMPMC), Sorbonne Universities, Paris VI University, CNRS UMR 7590, IRD UMR 206, MNHN, Paris.

5.1 - Introduction

Precise analysis of the distribution and crystallochemistry of the minerals present in soils and rocks from the Earth's surface contributes to what we know about the history and mechanisms of the chemical evolution of our planet. This analysis provides information on the formation of soils and how they function as well as on the geological CO_2 cycle, and on the conditions for formation of deposits of industrial minerals (kaolins) and ores, such as bauxite for aluminium or garnierite for nickel. The study of the processes by which rocks are altered is also important with a view to long-term storage of radioactive or industrial waste in sub-surface conditions.

The clay minerals formed by rock weathering contain paramagnetic impurities (transition ions) and point defects (radicals) of which EPR can identify and quantify a large number. This approach is illustrated here through recent studies performed on kaolinite-group minerals, which are found in numerous environments on the Earth's surface. After describing the structure of these minerals, we will present the EPR spectra of the Fe^{3+} ions which are often present as substituted impurities, and we will discuss the information that can be obtained.

P. Bertrand, *Electron Paramagnetic Resonance Spectroscopy*,
https://doi.org/10.1007/978-3-030-39668-8_5

We will also show that the paramagnetic defects generated in these minerals by natural radioactivity provide unique constraints by which to determine the conditions in which the minerals were formed, and in some cases, to date the weathering processes.

5.2 - Kaolinite-group minerals

Kaolinite, for which the ideal formula is $Al_2Si_2O_5(OH)_4$, is a type of clay, layered silicate minerals made of very small crystallites (typical size: around one micrometer). Kaolinite can be found in a wide variety of environments, such as tropical soils, sedimentary basins and hydrothermal systems; it is also an important industrial mineral, used in three main sectors: paper and cardboard manufacturing (up to 55 % by mass); ceramics and refractory industries, and reinforcement of plastomeres and elastomeres (up to 80 % by volume). The need to handle the crystallochemical variability of kaolinites to optimise their use has triggered numerous studies of their optical, morphological and crystallochemical properties [Cases *et al.*, 1982] as well as the products of their thermal transformations [Djemai *et al.*, 2001].

The triclinic structure of kaolinite [Bish and Von Dreele, 1989; Bish, 1993] is based on a layer made of two sheets: a sheet (T) of tetrahedral SiO_4 silicates linked by their vertex corners, bound through oxygen atoms to a sheet (O) of $AlO_2(OH)_4$ octahedra linked by their edges. In the latter, only two of the three possible octahedral sites are occupied (dioctahedral nature of the layer) (figure 5.1). Adjustment of the (T) and (O) sheets and the dioctahedral character result in distortion of the coordination polyhedra [Bailey, 1988].

In particular, the two non-equivalent octahedral sites noted Al_1 and Al_2 are compressed in the direction perpendicular to the layer. The coherence of assembly of the (TO) layers is ensured by hydrogen bonds between the OH^- hydroxides in the upper plane of the $AlO_2(OH)_4$ octahedra and the oxygens from the basal plane of the SiO_4 tetrahedra. Kaolinite naturally exists in powdered form, with a crystallite size of around the μm.

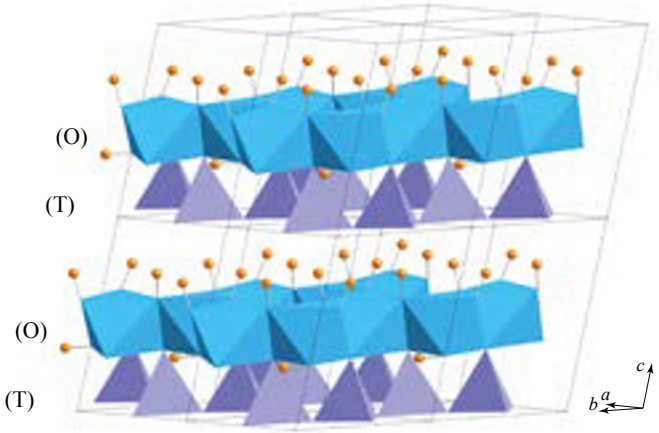

Figure 5.1 - Structure of kaolinite $Al_2Si_2O_5(OH)_4$. The structure results from the stacking of layers (2 layers are shown in the figure), each of which consists of a sheet of tetrahedral silicates and a sheet of octahedra centred on Al^{3+} ions. Three non-equivalent OH^- groups from octahedra, oriented sub-parallel to the c^* direction perpendicular to the layers, form hydrogen bonds with the oxygen of the tetrahedra from the adjacent layer.

Two polymorphous minerals of kaolinite exist with different stacking sequences for the TO layers:

- *Dickite* is formed in hydrothermal conditions or sedimentary basins [Beaufort *et al.*, 1998]. Its monoclinic cell it two-fold larger than kaolinite along the *c* axis, as one of the layers is the symmetric equivalent to the other due to the existence of a vertical glide plane [Bish and Johnston, 1993]. The hydroxides arrangement and distortion of the octahedral sites of dickite are slightly different from those reported for kaolinite.
- *nacrite* is a rare mineral formed in hydrothermal conditions [Buatier *et al.*, 1996]. It also has a double cell, but the stacking of the layers differs from that of kaolinite and dickite in that none of the SiO_4 tetrahedra from a layer face the $AlO_2(OH)_4$ octahedra of the adjacent layer [Giese, 1988].

Natural kaolinites present structural defects. Like in other layered silicates, the most frequent defects correspond to stacking defects, i.e., a succession of layers which, while maintaining inter-layer binding, does not reproduce the elements of symmetry (translations) of the ideal structure. The nature and proportions of stacking defects in kaolinites have been extensively debated, but no consensus has yet been reached [Bailey, 1988; Giese, 1988; Bookin *et al.,* 1989; Plançon *et al.,* 1989; Artioli *et al.*, 1995; Kogure and Inoue, 2005]. The most frequent

chemical impurity detected in kaolinites is iron, which is incorporated during growth of crystallites from aqueous solutions [Herbillon *et al.*, 1976; Mestdagh *et al.*, 1982]. Its presence in natural samples is often associated with a reduction in the size of the crystallites and an increased proportion of stacking defects [Brindley *et al.*, 1986].

5.3 - Fe^{3+} centres in kaolinite-group minerals

EPR spectroscopy has shown that Fe^{3+} ions substitute for Al^{3+} in the dioctahedral layers of natural kaolinites [Meads and Malden, 1975; Bonnin *et al.*, 1982; Brindley *et al.*, 1986; Muller and Calas, 1993; Gaite *et al.*, 1993, 1997; Delineau *et al.*, 1994]. As kaolinite is found as a powder, it is impossible to determine the orientation of the principal axes of the zero-field splitting matrix for the Fe^{3+} sites [Volume 1, section 6.2] relative to the crystallographic axes. This limitation makes the EPR approach less discriminative than in the case of single crystal samples, which explains why the number and characteristics (distribution, symmetry) of the substitution sites have long been the subject of controversy. X-band EPR spectra of Fe^{3+} centres in kaolinite-group minerals vary as a function of the polymorph studied and the degree of order in the samples. In the case of kaolinite, three signals are observed, noted $Fe_{(II)A}$, $Fe_{(II)B}$ and $Fe_{(I)}$ (figure 5.2):

- the $Fe_{(II)A}$ and $Fe_{(II)B}$ signals are produced by Fe^{3+} ions located in the two octahedral sites normally occupied by Al^{3+}. They most frequently appear in the form of a single spectrum noted $Fe_{(II)}$ and can only be distinguished in particularly well-ordered kaolinite samples (see section 5.3.2),
- the $Fe_{(I)}$ signal is characterised by a quasi-symmetric structure at $g \approx 4.3$ (150 mT at X-band). Its origin has been extensively debated [Meads and Malden, 1975; Brindley *et al.*, 1986; Gaite *et al.*, 1993, 1997] and we will see below how it is currently interpreted.

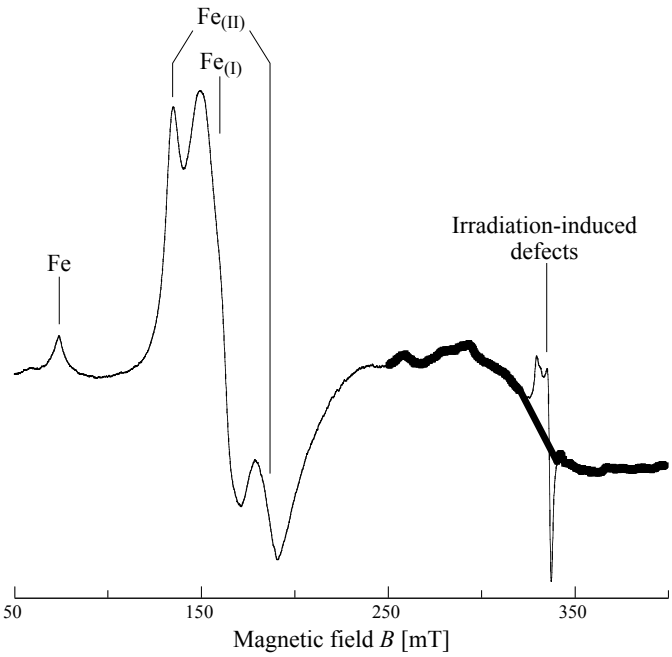

Figure 5.2 - X-band EPR spectrum (9.42 GHz) for a sample of natural kaolinite. The spectrum presents characteristic signals of structural Fe^{3+} ions substituted for Al^{3+} ions, of electronic defects induced by irradiation (A centres, see section 5.4), and a broad signal (highlighted part) centred at $g \approx 2$ produced by concentrated superparamagnetic iron phases (see section 5.3.2). The spectra were recorded on an ESP 300E spectrometer at room temperature. Power: 40 mW, modulation: frequency 100 kHz, peak-to-peak amplitude 0.5 mT.

5.3.1 - Interpretation of EPR signals for Fe^{3+} centres

◇ Sample preparation

Natural samples are subjected to granulometric sorting to eliminate the sandy fraction – mainly composed of quartz – and in some cases to chemical treatment (citrate-bicarbonate-dithionite) to selectively dissolve the iron oxides associated with kaolinite [Mehra and Jackson, 1960]. After heating, a constant sample volume is placed in a silica tube (Suprasil) and its weight (around 40 mg) is determined by double weighting for X-band analysis. For Q-band analysis, the sample volume is much smaller and the amount needs not be precisely determined.

◇ *Model of spectrum simulation*

To be able to apply EPR to the study of finely-divided minerals from soils required the development of a computational code to effectively simulate the spectra for polycrystalline samples. The ZFSFIT (*Zero-Field Splitting FITting*) code written by G. Morin and D. Bonnin [Morin and Bonnin, 1999] can calculate spectra from a spin Hamiltonian (spin $S \leq 5/2$) including second order (parameters D, E) and fourth order zero-field splitting terms, and sometimes hyperfine interaction terms (nuclei of spin $I \leq 7/2$). The theoretical bases and the calculation method are described in detail in [Morin and Bonnin, 1999]. This code presents numerous advantages compared to older algorithms [Gaite *et al.*, 1993; Chachaty and Soulié, 1995; Wang and Hanson, 1995]:

- ▹ Numerical diagonalisation of the spin Hamiltonian, already used by [Gaite *et al.,* 1993; Wang and Hanson, 1995], can be used to treat cases where perturbation theory cannot be applied due to comparable Zeeman and zero-field splitting terms. This situation is frequently encountered in the case of metal centres [Volume 1, section 9.5]. In addition, this method allows fourth-order zero-field splitting terms to be taken into account, which are very sensitive to the local symmetry of the ligand field. Hyperfine interactions are treated by second order perturbation theory when this approximation is valid. Otherwise, they are dealt with by complete diagonalisation.
- ▹ The calculation durations are reduced to a few seconds or minutes thanks to a triangular partition of the integration sphere, inspired by the very effective method developed to simulate NMR spectra [Aldermann *et al.,* 1986].
- ▹ Another novelty of the ZFSFIT code relates to the treatment of linewidth: inhomogeneous broadening due to fluctuations in the geometry of the paramagnetic centre in the polycrystalline material is simulated by introducing a distribution of the spin Hamiltonian parameters [Volume 1, section 9.5.3]. Indeed, studies carried out on the incorporation of Fe^{3+} and Cr^{3+} as substitutes for Al^{3+} in various minerals showed that it is essential to include a distribution of the zero-field splitting parameters in the calculation to correctly simulate the EPR spectra of natural minerals which generally present point defects or more extended defects [Morin and Bonnin, 1999; Balan *et al.,* 1999, 2000, 2002].

The ZFSFIT code was successfully used to identify the substitution sites for Fe^{3+} in aluminium (oxy)hydroxides such as gibbsite, α-$Al(OH)_3$ and boehmite, γ-AlOOH [Morin and Bonnin, 1999]. Here, it allows analysis of the process

by which Fe^{3+} has been incorporated into kaolinite-group minerals as well as of some irradiation-induced defects in phyllosilicates [Sorieul *et al.,* 2005].

◇ $Fe_{(II)}$-type signals: a characteristic of well-ordered samples

Simulation of the X-band and Q-band spectra for samples of kaolinite and dickite with exceptional crystallographic qualities made it possible to determine the zero-field splitting parameters for the sites producing the $Fe_{(II)A}$ and $Fe_{(II)B}$ signals (noted $Fe_{(D)A}$ and $Fe_{(D)B}$ for dickite). In figure 5.3 we show examples of kaolinite spectra and their simulations, and in table 5.1 we have listed the zero-field splitting parameters deduced from all the simulations [Balan *et al.*, 1999]. Spectra were simulated at several frequencies and several temperatures to determine these parameters with a high degree of precision. It should be noted that taking the fourth-order zero-field splitting parameters into account improves characterisation of the sites compared to results presented in a previous study [Gaite *et al.*, 1993].

The differences between the parameters obtained for kaolinite and dickite are due to relaxation of the internal structure of the layer linked to differences in stacking type (section 5.2). A study of iron-containing nacrite samples would complete this analysis of the relation between the stacking type and the relaxation of the dioctahedral layer. Unfortunately, none of the nacrite samples analysed up to now produce signals that could be attributed to Fe^{3+} centres.

Figure 5.3 - X- **(a)** and Q-band EPR spectra **(b)** for an exceptionally well crystallised sample of kaolinite from Decazeville. Spectra were recorded on an ESP 300E spectrometer **(a)** Power: 40 mW, modulation: frequency 100 kHz, peak-to-peak amplitude 0.5 mT. **(b)** Power: 40 mW, modulation: frequency 100 kHz, peak-to-peak amplitude 1 mT. Simulations allowed features produced by the $Fe_{(II)A}$ and $Fe_{(II)B}$ signals to be identified. The temperature-dependence of the spectrum indicates its sensitivity to minor structural variations.

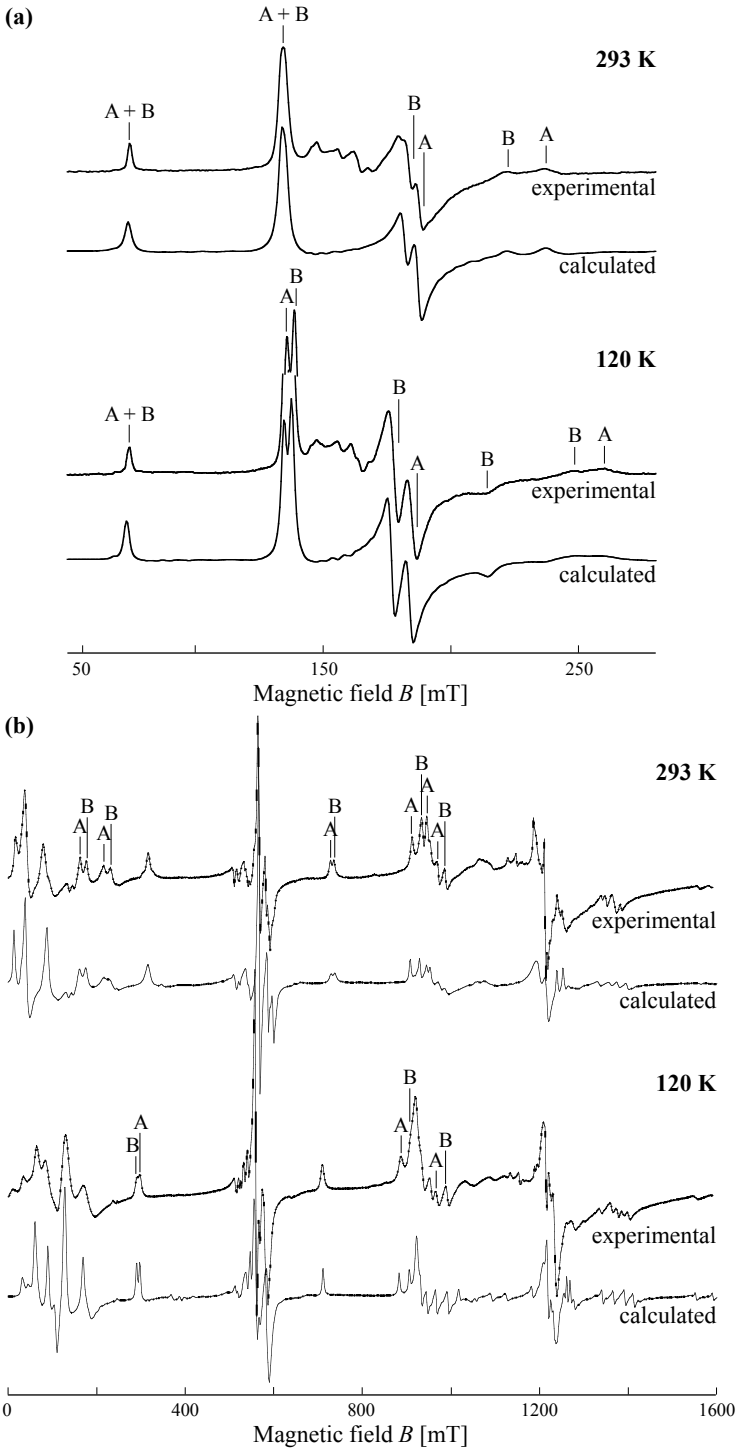
(a)
293 K
A + B
B
A
B
A
experimental
calculated
120 K
B
A
B
A + B
B
A
B
A
experimental
calculated
50
150
250
Magnetic field B [mT]
(b)
293 K
B
A
B
A
B
A
B
A
B
A
experimental
calculated
120 K
A
B
B
A
B
A
experimental
calculated
0
400
800
1200
1600
Magnetic field B [mT]

The EPR spectrum was also observed to be sensitive to the type of stacking in the case of Cr^{3+} ions. These ions are less commonly encountered than Fe^{3+}, but they have been observed to substitute for Al^{3+} ions in octahedral sites in samples of kaolinite and dickite from hydrothemal deposits [Balan *et al.*, 2002].

Table 5.1 - Zero-field splitting parameters for Fe^{3+} sites in kaolinite group minerals deduced from numerical simulations of $Fe_{(II)}$-type signals. $g = 2.00$ was assumed in the simulations.

Mineral	Temperature	Signal	D [cm^{-1}]	E [cm^{-1}]
kaolinite	293 K	$Fe_{(II)A}$	0.3312	0.0666
		$Fe_{(II)B}$	0.3171	0.0661
	120 K	$Fe_{(II)A}$	0.3468	0.0721
		$Fe_{(II)B}$	0.3360	0.0753
	4 K	$Fe_{(II)A}$	0.3594	0.0739
		$Fe_{(II)B}$	0.3450	0.0768
dickite	293 K	$Fe_{(D)A}$	0.3252	0.0851
		$Fe_{(D)B}$	0.3654	0.0993
	120 K	$Fe_{(D)A}$	0.3438	0.0901
		$Fe_{(D)B}$	0.3837	0.1031

◇ *EPR spectrum for a disordered sample: origin of the $Fe_{(I)}$-type spectrum*

When cations from transition elements are inserted into very disordered structures, their EPR spectrum cannot be simulated with a single set of zero-field splitting parameters: a broad, or even multimodal, distribution of these parameters is required [Kliava, 1986]. An inversion method with constraints can be used to deduce this distribution from the experimental spectrum, by discretisation of the second order zero field splitting parameters [Balan *et al.,* 1999]: the spectra corresponding to the nodes on a grid of zero-field splitting parameters can be calculated using the ZFSSIT code and the spectrum for the disordered material can be obtained by performing a weighted sum of the spectra. The weighting factors correspond to the distribution sought. Simultaneous inversion of experimental data acquired at X- and Q-band can be used to determine this distribution.

For some samples of disordered kaolinites, the distribution of the zero-field splitting parameters is multimodal (figure 5.4). One of the modes basically corresponds to the characteristic parameters of the octahedral sites of the ordered *kaolinite* ($Fe_{(II)}$ signals) and the two others to the parameters of the octahedral sites of dickite ($Fe_{(D)A}$ and $Fe_{(D)B}$ signals) (see table 5.1). Therefore, in these samples, local dickite-type

stacking very probably exists. This result is also suggested by infrared spectroscopy and X-ray diffraction experiments [Balan *et al.*, 2002, 2011]. However, other samples of disordered kaolinite, in particular those collected in lateritic soils from Cameroon, do not display this multimodal distribution [Balan *et al.*, 2011]. Thus, several types of disorder are possible in kaolinite-group minerals. The relations between these types of disorder and the growth conditions for the crystallites remain to be determined.

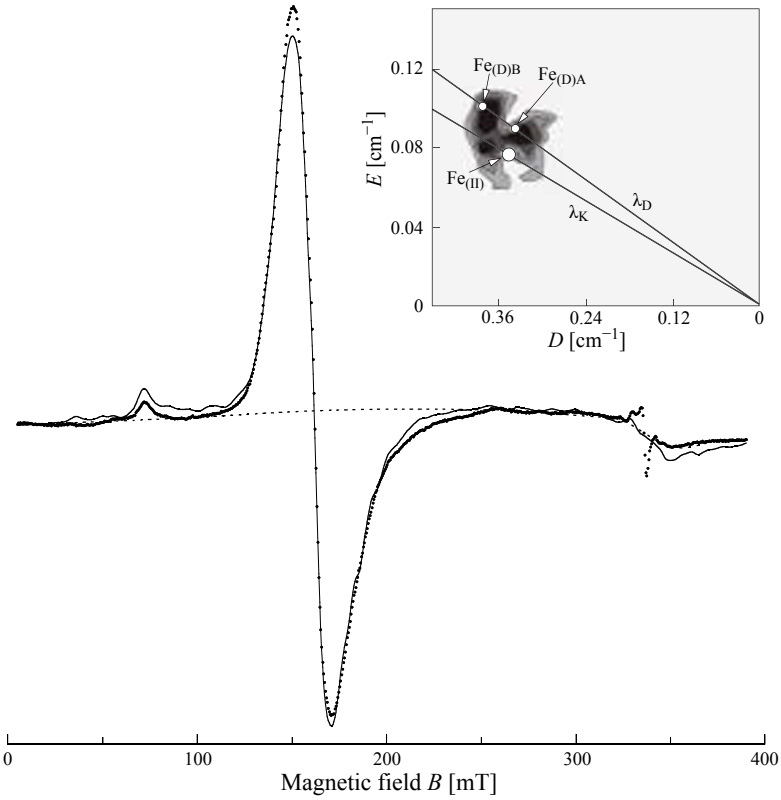

Figure 5.4 - X-band EPR spectrum (dotted lines) for a sample of disordered kaolinite sampled at the top of a lateritic profile in the region of Manaus (Brazil) (sample B4 in figure 5.7). Same experimental conditions as in figure 5.2. The spectrum is dominated by an $Fe_{(I)}$-type signal. The inset shows the distribution of the (D, E) parameters deduced from the simulation (continuous line). The grey scale reflects the values of the weighting factors (see text). The distribution includes three modes centred on values close to those characterising the $Fe_{(II)}$ signals for kaolinite and $Fe_{(D)A}$, $Fe_{(D)B}$ for dickite (table 5.1), indicated by white circles. The small shift is probably linked to the fact that the fourth-order zero-field splitting parameters were not taken into consideration in the simulation. The straight lines shown in the inset indicate that the shift occurs at constant rhombicity ($\lambda = E/D$).

5.3.2 - Determining the absolute concentration of structural iron

To interpret the EPR spectrum for Fe^{3+} ions substituted into kaolinites, we implicitly assumed them to reliably reflect the crystal order of the samples. This is only true if these ions are present at sufficiently high concentrations and if they are distributed homogeneously within the crystallites. This is a first reason to determine the concentration of the Fe^{3+} ions producing the EPR spectrum. Another reason is that comparison of this concentration to that of the total iron contained in the sample supplies information on the physicochemical conditions of the medium where the kaolinites grew [Muller *et al.*, 1995].

To determine the concentration of Fe^{3+} ions, the simplest method consists in comparing the intensity of the experimental spectrum to that produced by a reference kaolinite with a known Fe^{3+} concentration (for intensity measurements, see Volume 1, complement 4 to chapter 9). Unfortunately, all natural or synthetic samples of iron-containing kaolinites contain concentrated iron phases, which can be detected by diffuse reflectance spectroscopy [Malengreau *et al.*, 1994] or thanks to their super-paramagnetic resonance signal [Bonnin *et al.*, 1982]. In contrast, the incorporation of Fe^{3+} at high temperature and low concentrations in corindon α-Al_2O_3 occurs homogeneously, generating a system where the Fe^{3+} ions are diluted [De Biasi and Rodrigues, 1983]. A sample of corindon containing Fe^{3+} ions can therefore be used as a standard since the intensity of its EPR spectrum is proportional to the concentration measured by chemical analysis. The EPR spectra for Fe^{3+} centres in kaolinite and corindon are different, but the parameters of the spin Hamiltonian are known in both cases. Calibration can thus be performed by *calculating* the EPR spectra produced by the same quantity of Fe^{3+} ions in kaolinite and the standard. The concentrations of Fe^{3+} ions measured in this way in samples collected at different sites (France, England, Cameroon, Brazil) vary between a few hundreds of ppm and around 3,000 ppm for kaolinites from the Amazonian basin [Balan *et al.*, 2000].

This information can be used to determine how the iron is distributed between Fe^{3+} ions diluted in the structure of the kaolinite and other forms of iron which are not quantifiable by EPR and resist selective chemical dissolution treatments [Mehra and Jackson, 1960]. These other forms can be substituted Fe^{2+} ions, or more frequently, closely-spaced Fe^{3+} ions: aggregates of Fe^{3+} ions substituted into the dioctahedral kaolinite layer [Schroeder and Pruett, 1996] or super-paramagnetic nano-phases of iron oxides or oxyhydroxides [Malengreau *et al.*,

1994]. Magnetic resonance cannot distinguish between these phases, which both produce a broad signal at around $g = 2$ at X-band (figure 5.2) (see Volume 1, section 7.4 for the EPR spectrum of aggregates, and chapter 12 of this volume for the FMR of super-paramagnetic particles). The total iron concentration measured by chemical analysis varies between 2000 and 8000 ppm, depending on the origin of the kaolinites. Comparison with the concentrations measured by EPR reveals that in the samples studied, dilute structural Fe^{3+} represents less than half of the total iron, which demonstrates that iron preferentially forms concentrated phases during kaolinite growth. The concentration of the dilute structural Fe^{3+} and the disordered nature of the samples are apparently not correlated [Balan *et al.*, 2000].

EPR has also been used to study other transition elements present in minerals in the kaolinite group, such as vanadium, chromium and manganese. In the cases of manganese and vanadium, identification of specific species (Mn^{2+} and VO^{2+}) reflects the specific reduction-oxidation conditions which prevailed during formation of the kaolinites [Muller *et al.*, 1993, 1995; Allard *et al.*, 1997].

5.4 - Paramagnetic defects produced by irradiation

The first paramagnetic defects due to natural irradiation of kaolinites were identified in the 1970s [Angel *et al.*, 1974]. Three types are now known to exist; they are all electronic holes localised on oxygen atoms, but are distinguished by their atomic environment, the orientation of the orbital occupied by the unpaired electron, and their thermal stability. We can thus distinguish A centres, A' centres and B centres [Clozel *et al.*, 1994] (figure 5.5).

A centres are generally the most abundant and are thus used for geological applications as they are stable over the timescales involved. Indeed, the half-life of these centres is around 10^{12} years at room temperature [Clozel *et al.*, 1994]. A centres can be modelled as an electronic hole which compensates the charge imbalance appearing when divalent ions such as Mg^{2+} are substituted for Al^{3+}. The unpaired electron from the oxygen is located in the π orbital of an $Si–O_{apical}$ bond.

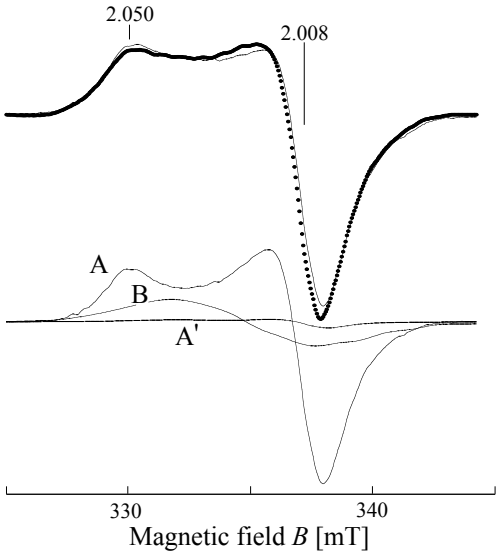

Figure 5.5 - Simulation of the X-band spectrum for the irradiation-induced defects in a kaolinite from the region of Manaus, showing the predominance of the signal due to A centres. Power: 40 mW, modulation: frequency 100 kHz, peak-to-peak amplitude 0.3 mT.

A centres are mainly produced by α, β, or γ ionising radiation. Their EPR signal has been used in several studies related to Earth sciences:

- ▹ to record past radioactivity in iron-containing nodules from lateritic profiles [Muller and Calas, 1989],
- ▹ to reveal past migrations of radio elements [Muller *et al.*, 1990, 1992; Ildefonse *et al.*, 1990, 1991] and quantify them [Allard and Muller, 1998; Allard *et al.*, 2007].

In section 5.5.3 we will see that the signal for an A centre can also be used to *date* kaolinites from soils and sediments from tropical areas [Balan *et al.*, 2005].

It should be noted that dickite, a polymorph of kaolinite (section 5.2), contains similar defects [Allard *et al.*, 2003]. The effects of irradiation are now known for various clays [Allard and Calas, 2009] and the recent discovery of irradiation-induced defects in clays such as *smectite, illite* and *sudoite* will make study of new geological environments possible [Sorieul *et al.*, 2005; Morichon *et al.*, 2008, 2010a, b].

5.5 - Application of kaolinite EPR to the study of weathering processes in tropical climates

5.5.1 - Alteration and formation of tropical soils

Tropical soils cover more than one third of the surface of emerged continents, and almost half of the world's continental water flow filters through these soils before entering the ocean [Tardy, 1993; Tardy and Roquin 1998]. These soils are produced by *geochemical alteration* of the continental crust, which consists in dissolving primary minerals and formation of less soluble minerals which accumulate within the soils. These minerals, formed at the Earth's surface, are mainly clay minerals and iron or aluminium oxides or hydroxides. For example, dissolution of the common feldspar, orthoclase, in acidic conditions can result in the formation of kaolinite and the leaching of soluble ions and molecules (in this case potassium and orthosilicic acid) into the hydrosphere:

$$2(Si_3AlO_8K)_{solid} + 9H_2O + 2H^+ \rightleftarrows (Si_2Al_2O_5(OH)_4)_{solid} + 2(K^+)_{aq} + 4(H_4SiO_4)_{aq} \quad [5.1]$$

The conditions of tropical alteration combine a high mean temperature, a high volume of precipitation and a high rate of biological production. These factors accelerate mineral dissolution, and tropical soils can be counted among the most altered media on the Earth's surface; their history may extend over several million years. It includes the evolution of the physicochemical conditions linked to climate variations and changes to the landscape [Muller and Calas, 1989; Girard *et al.*, 2000; Braun *et al.*, 2005] while also involving the link between chemical reactions and transport of reagents [Nahon and Merino, 1996]. The resulting structural and textural complexity must be deciphered to elucidate the role played by each mechanism.

In profiles of lateritic soils, clay minerals and iron oxides often present significant variations in size, chemical composition and structural order from the bottom to the top of the profile, indicating dissolution of ancient populations and crystallisation of more recent ones. At each level, minerals inherited from ancient populations and neoformed minerals are therefore likely to be observed in proportions which depend on the rate of dissolution and crystallisation. Depending on the hypotheses used to determine these rates, several evolutionary scenarios can be proposed for the systems:

- If we assume that dissolution and recrystallisation are rapid, the fraction of inherited materials will be low. In this case, the crystallochemical and isotopic characteristics observed are assumed to reflect the physicochemical conditions currently prevailing in the environments studied. Heterogeneity of the mineral populations is attributed to spatial or physicochemical fluctuations in these physicochemical conditions, linked for example to the coexistence of distinct micro-environments or to seasonal fluctuations in rainfall [*e.g.* Giral-Kacmarcik *et al.*, 1998].
- Conversely, if mineral transformation is slow, the fraction of inherited minerals will be high, and the minerals in the soil are likely to preserve the memory of ancient conditions, or even traces of continental palaeoclimates [Girard *et al.*, 2000].

The capacity of lateritic profiles to preserve an ancient message is attested by manganese oxides detected in lateritic crusts from West Africa and Brazil which were dated at more than 40 Ma [Henocque *et al.*, 1998]. Magnetostratigraphic experiments performed on profiles from French Guyana [Théveniaut and Freyssinet, 1999] also indicate ancient epochs. However, other approaches, such as dating based on uranium and thorium decay chains [Mathieu *et al.*, 1995; Dequincey *et al.*, 1999; Chabaux *et al.*, 2003a, b] and the radioactive isotopes produced by cosmic radiation such as ^{10}Be [Brown *et al.*, 1994], indicate more recent emergence, with ages of less than 2 Ma, or even 0.3 Ma in certain studies. This partial view of the history of lateritic profiles can also be explained by the fact that there is currently no general method to date successive generations of minerals neoformed during the different weathering processes involved. Interpretation of observations performed on mobile soil horizons is even more delicate. Indeed, the small size of the minerals observed and the circulation of fluids may lead to rapid evolution of these minerals.

In this context, EPR study of kaolinites can allow us to distinguish several populations using signals for Fe^{3+} centres to probe the local order of their structure, while also estimating their age by quantifying signals due to the paramagnetic defects induced by natural radioactivity.

5.5.2 - Tracing kaolinite generations in tropical soils using Fe^{3+} EPR

Kaolinites were sampled vertically throughout a section of lateritic soil from the centre of the Amazonian basin, in the region around Manaus (figure 5.6), and their X-band EPR spectra were recorded (figure 5.7). The characteristic spectral

features of $Fe_{(II)}$ signals, typical of well-ordered kaolinites (figure 5.3a), and $Fe_{(I)}$, typical of disordered kaolinites were observed (figure 5.4). The relative proportions of the two signals varied throughout the profile, in a direction indicating an increase in crystal disorder from the bottom to the top. This increase in disorder correlates with a reduction in the size of the particles, as measured by granulometric sorting [Fritsch *et al.*, 2002].

Figure 5.6 - Vertical section showing the different horizons of a lateritic soil from the Manaus region. Samples were collected at the seven levels indicated by the circles. The structures observed on the section (discolouration, indurated iron-oxide-rich line) reflect recent re-mobilisation of iron due to fluctuations in the reduction-oxidation conditions which did not affect the kaolinites.

A more quantitative analysis reveals that the spectra are the result of a linear combination of two reference spectra (figures 5.7 and 5.8):

- the first, A1, is that of a well-ordered kaolinite typical of the sediment. It is very similar to the spectrum shown in figure 5.3a,
- The other, B4, is due to a very disordered kaolinite, representative of the upper horizons of lateritic soils from the Manaus region. This is the spectrum shown in figure 5.4.

In section 5.3.1, we saw that the spectrum for the disordered sample presents a strong “dickite”-type component (see inset to figure 5.4) reflecting the existence of a high proportion of stacking defects. This interpretation is consistent with the fact that the infrared spectrum for this sample presents extensive similarities to that of dickite in the range of frequencies characteristic of the OH-stretching modes (see figure 5.1) [Balan *et al.*, 2002, 2011].

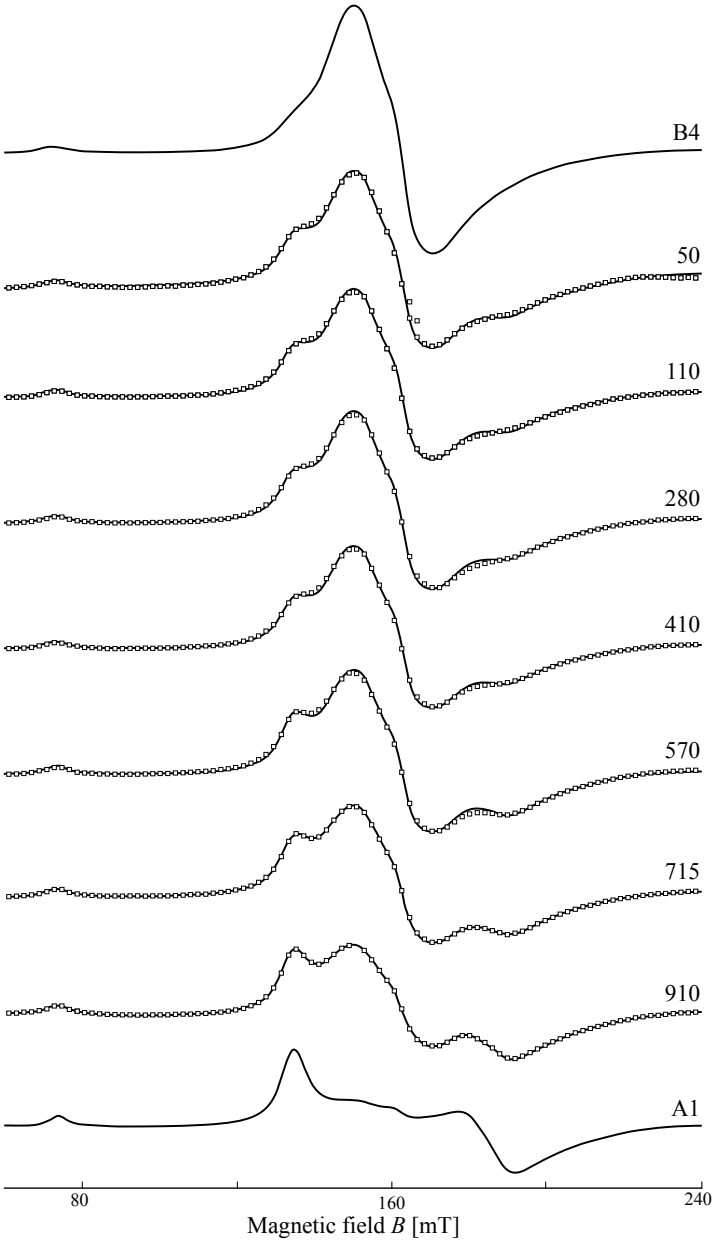

Figure 5.7 - X-band EPR spectra of structural Fe^{3+} ($Fe_{(I)}$ and $Fe_{(II)}$) for the seven samples of kaolinite collected from the profile shown in figure 5.6. The sampling depths are indicated in cm to the right of spectra. Experimental spectra are represented by dotted lines. The simulations obtained by linear combination of reference spectra A1 and B4, due to ordered and disordered samples, respectively, are represented by the continuous line. The experimental conditions are the same as those in figure 5.2.

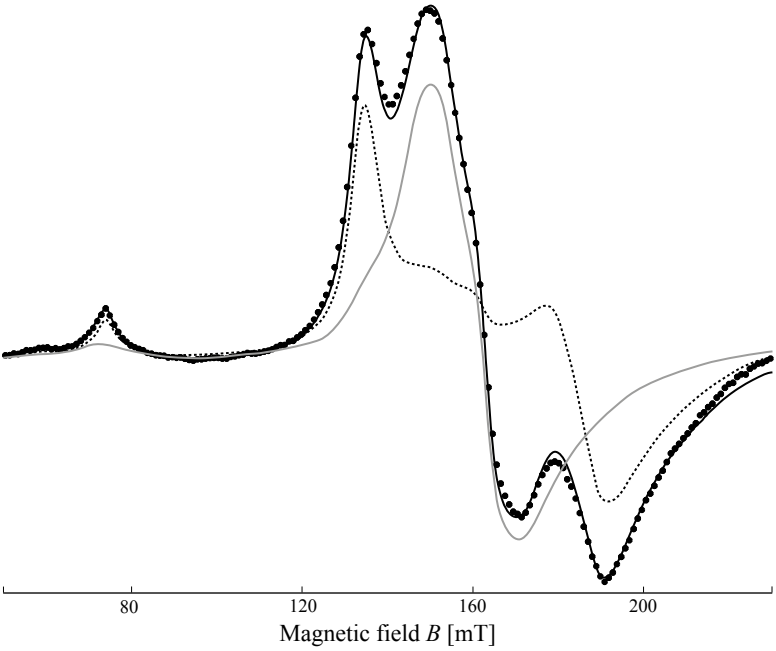

Figure 5.8 - EPR spectrum for the sample collected at 910 cm depth (black dots) and its simulation (continuous black line) obtained by linear combination of the A1 (black dashes) and B4 (continuous grey line) components.

The spectra for samples collected on the profile show that they contain a mixture of two types of kaolinites, an ordered one from sedimentary levels, and a disordered one typical of soil. Their relative proportions, deduced from simulations of the EPR spectra, are in very good agreement with those determined by infrared spectroscopy (figure 5.9).

The persistence of ordered kaolinite in the upper levels of the profile suggests a relatively slow rate of transformation of the kaolinites by dissolution/recrystallisation, and thus the presence of ancient kaolinite populations within lateritic profiles [Balan *et al.*, 2007].

In addition, the transformation of ordered kaolinite to produce disordered kaolinite appears to occur independently of other mineralogical transformations observed in the same lateritic profile, for example, transformation of iron oxides which was studied by Mössbauer spectroscopy, X-ray diffraction and diffuse reflectance UV-visible spectroscopy [Fritsch *et al.,* 2005]. Haematite (Fe_2O_3) and goethite (FeOOH) observed at the bottom of the profile are progressively replaced by aluminium-substituted goethite ($Fe_{0.67}Al_{0.33}OOH$) towards the top,

through a dissolution and re-precipitation reaction. This transformation, limited to the upper part of the alteration profiles, is superposed on that of the kaolinites but does not modify it; it occurred after the appearance of the disordered kaolinite populations. This more recent dissolution/recrystallisation of iron oxides can also lead, due to the vertical migration of Fe and Al, to individualised discoloured pockets at meter or hectometer scale. These pockets are limited at their base by fine iron-oxide-enriched levels (figure 5.6) [Fritsch *et al.*, 2002].

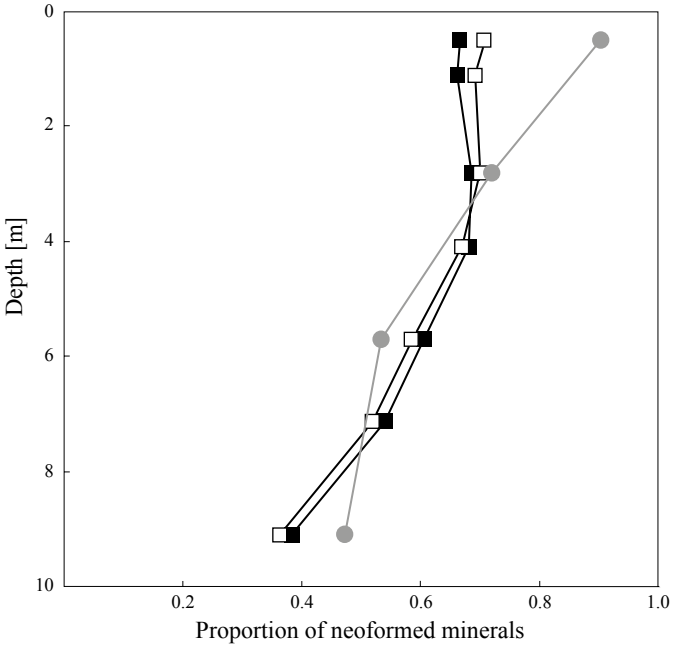

Figure 5.9 - Tracing the transformation of kaolinites throughout the profile shown in figure 5.6, as determined using EPR (white squares) and infrared (black squares) spectroscopies, superposed on the transformation of iron oxides as determined by Mössbauer spectroscopy (grey circles). Simulation of the spectra allows the replacement of older mineral populations by more recent ones to be quantified. The results show that the changes occurring in kaolinites and iron oxides are not synchronous.

5.5.3 - EPR-dating of kaolinites from lateritic soils

EPR can also be used to estimate the age of kaolinites. This approach was inspired by previous work in which the defects produced by irradiation of minerals from the kaolinite group were used to analyse the transfer of radionuclides in geological environments [Allard and Muller, 1998; Allard *et al.*, 2007]. The principle of EPR-dating is the same as that of the archaeological

dating described in detail in section 1.2 of chapter 1. We will simply indicate the specific elements used to date kaolinites from three sites in the Manaus region [Balan *et al.*, 2005].

◇ *Determining the palaeodose*

The irradiation dose recorded by kaolinite until now (palaeodose) was determined by using EPR to measure the concentration of irradiation-induced defects, which are mainly A centres (figure 5.5). The calibration curve, which links this concentration to the received dose, was obtained by performing artificial irradiation experiments. In these experiments, we used 1.5-MeV He^+ ions produced by the ARAMIS accelerator at the CSNSM from Université Paris-Sud, the characteristics of which are described in [Bernas *et al.*, 1992]. Two representative samples of ordered and disordered kaolinite were subjected to a large range of irradiation doses (figure 5.10).

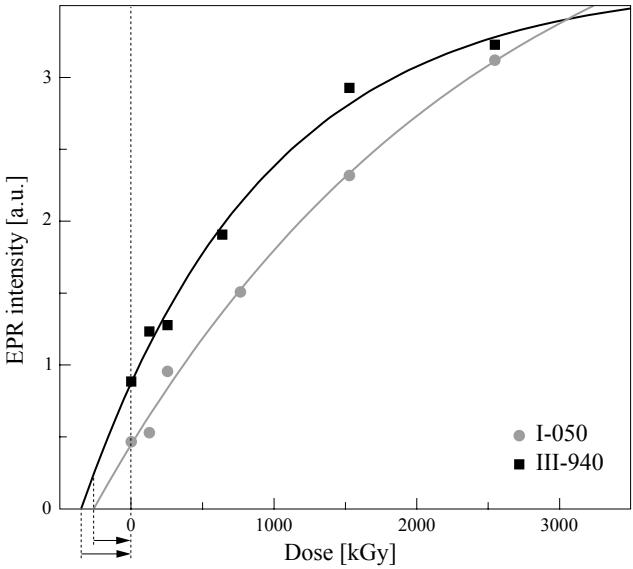

Figure 5.10 - Sensitivity curves obtained by irradiating two representative kaolinite samples from the Manaus region with 1.5-MeV He^+ ions. The ordinate represents the intensity of the signal for the A centre in arbitrary units. The arrows indicate the palaeodoses determined.

It should be noted that these doses are much larger than those used for carbonates or phosphates, which are around a kGy (figure 1.3 in chapter 1) [Ikeya, 1993] as it is more difficult to create irradiation defects in kaolinite than in these minerals.

The results are well described by the following equation, which is identical to equation [1.3] in chapter 1 [Grün, 1991; Allard *et al.*, 1994]:

$$I = I_0[1 - e^{-\mu(D+P)}] \quad [5.2]$$

where I is the intensity of the EPR signal, which is proportional to the concentration of the irradiation-induced defects, I_0 is the saturation intensity, D is the applied dose in grays (1 Gy = 1 J kg^{-1}), P is the palaeodose, and μ is the efficiency coefficient, which depends on the mineral studied and the type of radiation used.

The values of μ deduced from these studies (7.8×10^{-4} kGy^{-1} for the ordered sample and 3.7×10^{-4} kGy^{-1} for the disordered sample) were used to extrapolate the palaeodose for the other samples from the intensity of the signal for their defects. The palaeodoses obtained by this method varied between 100 and 1000 kGy (figure 5.12).

◇ *Determining the dose rate*

For stable defects like the A centre, the palaeodose is the integral of the dose rate over time since the formation of the kaolinites (equation [1.1] in chapter 1). To convert the palaeodose determined by EPR into an age, we must therefore know the rate of the dose recorded by the kaolinite and any variations it has undergone over time. The effect of cosmic radiation is considered negligible due to the depth at which these samples were collected. The *current* annual dose can be calculated from the concentration of the radioactive elements, mainly U and Th, contained in the samples studied. Alpha radiation, for which the depth of penetration in matter is around 10 μm, is known to efficiently create irradiation-induced defects. To determine its contribution to the dose rate, we must therefore analyse the spatial distribution of the radioactive elements in the soil samples:

- ▹ The spatial distribution of uranium was determined at the μm scale on thin sections using cartography of the induced fission traces (figure 5.11). These maps reveal that uranium is concentrated in zircon grains and that it is also present, to a lesser extent, in titanium and iron oxides. Given its shallow depth of penetration, it is likely that the alpha radiation produced by uranium decay chains contributes little to the dose recorded by the kaolinites, and its contribution was therefore omitted when determining the dose rate.

▹ The spatial distribution of thorium could not be analysed directly as no appropriate imaging method was available. Analysis of series of isolated zircon grains [Balan *et al.*, 2001] indicated that thorium is not a major element in these grains, and that it is probably diluted throughout the clay matrix. The corresponding dose of alpha radiation was therefore taken into account when calculating the dose rate.

A significant difficulty in dating soils is linked to the open geochemistry of these media, which is likely to cause the dose rate to vary. In the case of EPR dating, this may be due to uranium leaching, as this element is soluble, and therefore mobile, in oxidising conditions. In formations from the Manaus region, the concentration of uranium within zircons showing low self-irradiation damage (low degree of amorphisation) limited migration of this element, as indicated by the relatively constant ratio between the uranium and thorium concentrations; thorium has relatively low geochemical mobility due to its very low solubility. These observations suggest that the dose rate varied little over time. It was therefore considered constant, and equal to the current annual dose calculated.

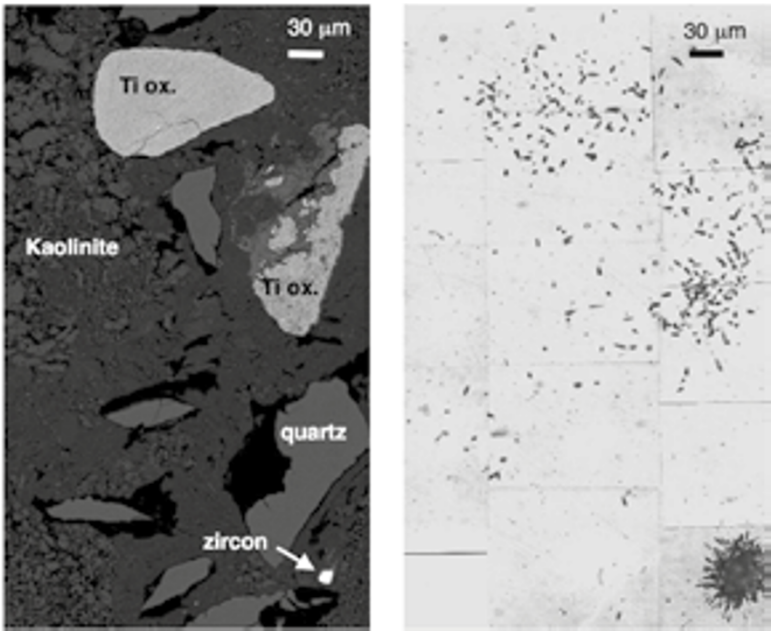

Figure 5.11 - Image obtained by scanning electron microscopy with backscattered electrons (left) and corresponding map of the traces of induced fission in uranium (right). Note the heterogeneous distribution of the uranium, which is mainly concentrated within the zircon grain (lower right) and within two larger-volume titanium oxides grains (top).

◇ *Age of kaolinites*

If we represent each sample of kaolinite by a point on a graph with the dose rate on the abscissa and the palaeodose as ordinate, the age of the sample will be given by the *slope* of the line joining this point to the origin (figure 5.12). The points representing kaolinite from sedimentary horizons practically align, suggesting that they are of similar age, slightly greater than 25 Ma. This result confirms that these kaolinites formed within the sediment by alteration of material initially deposited around the end of the Cretaceous period. Although more recent, kaolinite from the soil was found to have an age of around 6 to 10 Ma. This result appears to refute the rapid dissolution/recrystallisation model which would maintain them in equilibrium with current conditions in the medium (section 5.5.1).

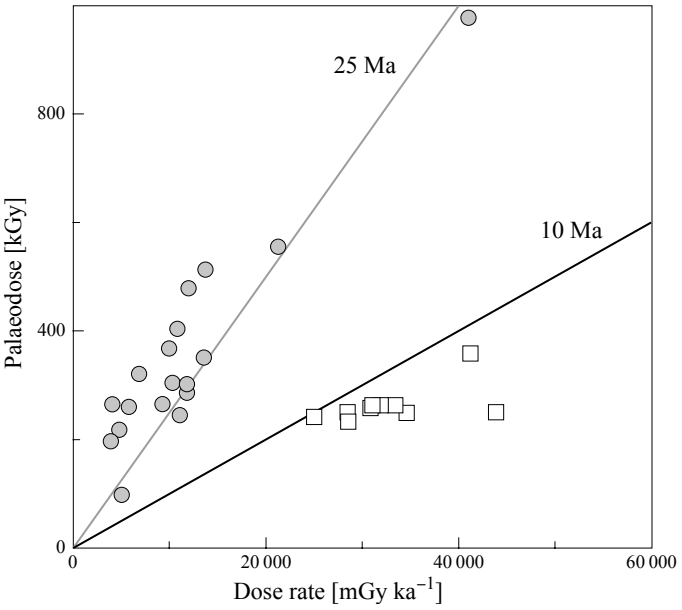

Figure 5.12 - Determining the age of kaolinite samples. Circles represent samples from sedimentary horizons and squares correspond to soil samples. If the dose rate is constant, the isochrone curves are straight lines passing through the origin. Although more recent than kaolinites from sediment, the significant concentration of irradiation defects observed in soil kaolinites reflects their old age.

The relative resistance of kaolinite to dissolution/precipitation at the Earth's surface is compatible with the ancient nature of the transformation of ordered kaolinite to produce disordered kaolinite, as observed vertically in soil profiles.

Through its composition in stable isotopes of oxygen and hydrogen, kaolinite is therefore likely to supply palaeoclimatic information. In contrast, a significant contribution of kaolinites to the rapid exchange of silica between the soil and plant coverage [*e.g.* Lucas *et al.*, 1993, 1996] is questionable, and the role of other silica-containing phases (*e.g.* biological silica) deserves to be investigated. It should be noted that the site of Manaus where this study was performed is exceptional in that it shows very limited migration of radioactive elements. Application of this method to profiles developed on endogenous rocks presenting several uranium-containing minerals, such as titanite ($CaTiSiO_5$) or monazite ($LaPO_4$), and potassium-containing minerals, such as micas, may therefore be much more difficult. In addition to the variation in dose rate, the presence of water in the system and the spatial distribution of radionuclides can lead to significant uncertainty in the age determined for kaolinites. This uncertainty can be minimised by studying samples collected in environments which may be dated by other methods.

5.6 - Conclusion

Despite the heterogeneity and variability of natural samples, their study by spectroscopic techniques sensitive to the local environment of the atoms and defects, such as EPR, reveals unexpected regularities at the atomic scale. Thus, thanks to its unique sensitivity, EPR can be used to obtain quantitative information on the structural order of the minerals, and on concentrations of defects and trace impurities. EPR can therefore provide very novel information, both on the formation media and on modifications to the environmental conditions.

The use of EPR to monitor ongoing environmental modifications due to chemical or radiological pollution constitutes a significantly underexploited field (nevertheless, see application described in chapter 2). EPR dating of minerals from soils constitutes another challenge with significant potential, and represents a unique possibility to quantify the historical evolution of continental surfaces, which is essential if we are to study historical climate change.

References

Alderman D. W. *et al.* (1986) *Journal of Chemical Physics* **84**: 3717-3725.

Allard T. *et al.* (1994) *Physics and Chemistry of Minerals* **21**: 85-96.

Allard Th. *et al.* (1997) *Comptes Rendus de l'Académie des Sciences Paris,* Série II, Sciences de la Terre et des Planètes. **325**: 1-10.

Allard T. & Muller J.-P. (1998) *Applied Geochemistry* **13**: 751-765.

Allard T. *et al.* (2003) *European Journal of Mineralogy* **15**: 629-640.

Allard Th., Ildefonse Ph. & Calas G. (2007) *Chemical Geology* **239**: 50-63.

Allard T. & Calas G. (2009) *Applied Clay Science* **43**: 143-149.

Angel B.R., Jones J.P.E. & Hall P.L. (1974) *Clay Minerals* **10**: 247-255.

Artioli G. *et al.* (1995) *Clays and Clay Minerals* **43**: 438-445.

Bailey S.W. (1988) "Introduction; polytypism of 1:1 layer silicates" in *Hydrous phyllosilicates (exclusive of micas)*, S.W. Bailey, ed., Reviews in Mineralogy, Mineralogical Society of America.

Balan E. *et al.* (1999) *Clays and Clay Minerals* **47**: 605-616.

Balan E. *et al.* (2000) *Clays and Clay Minerals* **48**: 439-445.

Balan E. *et al.* (2001) *American Mineralogist* **86**: 1025-1033.

Balan E. *et al.* (2002) *Physics and Chemistry of Minerals* **4**: 273-279.

Balan E. *et al.* (2005) *Geochimica et Cosmochimica Acta* **69**: 2193-2204.

Balan E. *et al.* (2007) *Clays and Clay Minerals* **55**: 253-259.

Balan E. *et al.* (2011) *Comptes Rendus Géoscience* 343: 177-187.

Beaufort D. *et al.* (1998) *Clay minerals* **33**: 297-316.

Bernas H. *et al.* (1992) *Nuclear Instruments and Methods in Physics Research* **B62**: 416-420.

Bish D.L. (1993) *Clays and Clay Minerals* **41**: 738-744.

Bish D.L. & Johnston C.T. (1993) *Clays and Clay Minerals* **41**: 297-304.

Bish D.L. & Von Dreele R.B. (1989) *Clays and Clay Minerals* **37**: 289-296.

Bonnin D., Muller S. & Calas G. (1982) *Bulletin de Minéralogie* **105**: 467-475.

Bookin A.S. *et al.* (1989) *Clays and Clay Minerals* **37**: 297-307.

Braun J.-J. *et al.* (2005) *Geochimica et Cosmochimica Acta* **69**: 357-387.

Brindley G.W. *et al.* (1986) *Clays and Clay Minerals* **34**: 239-249.

Brown E.T. *et al.* (1994) *Earth Planet Sci. Lett.* **124**: 19-33.

Buatier M.D. *et al.* (1996) *European Journal of Mineralogy* **8**: 847-852.

Calas G. (1988) « Electron paramagnetic resonance » in *Spectroscopic methods in mineralogy and geology.*, F.C. Hawthorne. ed., Reviews in Mineralogy, Mineralogical Society of America **18**: 513-571.

Cases J-M. *et al.* (1982) *Bulletin de Minéralogie* **105**: 439-455.

Chabaux F., Riotte J. & Dequincey O. (2003) (a) *Reviews in Mineralogy and Geochemistry* **52**: 533-576.

Chabaux F. *et al*. (2003) (b) *Comptes Rendus Géoscience* **335**: 1219-1231.

Chachaty C. & Soulié E. J. (1995) *Journal de Physique III France* **5**: 1927-1952.

Clozel B., Allard Th. & Muller J-P. (1994) *Clays and Clay Minerals* **46**: 657-666.

De Biasi R.S. & Rodrigues D.C.S. (1983) *Journal of Material Science Letters* **2**: 210-212.

Delineau T. *et al.* (1994) *Clays and Clay Minerals* **42**: 308-320.

Dequincey O. *et al.* (2002) *Geochim. Cosmochim. Acta* **66**: 1197-1210.

Djemai A. *et al.* (2001) *Journal of the American Ceramic Society* **84**: 1017-1024.

Fritsch E. *et al.* (2002) *European Journal of Soil Science*, **53**: 203-218.

Fritsch E. *et al.* (2005) *European Journal of Soil Science* **56**: 575-588.

Gaite J-M., Ermakoff P. & Muller J-P. (1993) *Physics and Chemistry of Minerals* **20**: 242-247.

Gaite J-M. *et al.* (1997) *Clays and Clay Minerals* **45**: 496-505.

Giese R.F., Jr (1988) « Kaolin Minerals: Structures and Stabilities » in *Hydrous phyllosilicates (exclusive of micas)*, S.W. Bailey, ed., Reviews in Mineralogy, Mineralogical Society of America **19**, 725 pp.

Giral-Kacmarcik S. *et al.* (1998) *Geochimica et Cosmochimica Acta* **62**: 1865-1879.

Girard J.-P., Freyssinet Ph. & Chazot G. (2000) *Geochimica et Cosmochimica Acta* **64**: 409-426.

Grün R. (1991) *Nuclear Tracks and Radiation Measurements* **18** (1/2): 143-153.

Henocque O. *et al.* (1998) *Geochimica and Cosmochimica Acta* **62**: 2739-2756.

Herbillon A. J. *et al.* (1976) *Clay Minerals* **11**: 201-220.

Ikeya M. (1993) *New applications of electron spin resonance - Dating, Dosimetry and Microscopy*, World Scientific Publishing, Singapore.

Ildefonse P. *et al.* (1991) *Material Research Society Symposium Proceedings* vol 749-756.

Ildefonse P. *et al.* (1990) *Economic Geology* **29**: 413-439.

Kliava J. (1986) *Physica Status Solidi B* **134**: 411-455.

Kogure T. & Inoue A. (2005) *European Journal of Mineralogy* **17**: 465-473.

Lucas Y. *et al*. (1993) *Science* **260**: 521-523.

Lucas Y. *et al*. (1996) *Comptes Rendus de l'Académie des Sciences de Paris* **322**: 1-16.

Malengreau N., Muller J.-P. & Calas G. (1994) *Clays and Clay Minerals* **42**: 137-147.

Mathieu D., Bernat M. & Nahon D. (1995) *Earth and Planetary Science Letters* **136**: 703-714.

Meads R.E. & Malden P.J. (1975) *Clay Minerals* **10**: 313-345.

Mehra O.P. & Jackson M.L. (1960) *Clays and Clay Minerals* **7**: 317-327.

Mestdagh M.M. *et al.* (1982) *Bulletin de Minéralogie* **105**: 457-466.

Morichon E. *et al.* (2008) *Physics and Chemistry of Minerals* **35**: 339-346

Morichon E. *et al*. (2010) (a) *Physics and Chemistry of Minerals* **37**: 145-152.

Morichon E. *et al.* (2010) (b) *Geology* **38**: 983-986.

Morin G. & Bonnin D. (1999) *Journal of Magnetic Resonance* **136**: 176-199.

Muller J.P. & Calas G. (1989) *Economic Geology* **84**: 694-707.

Muller J.P., Ildefonse P. & Calas G. (1990) *Clays and Clay Minerals* **38**: 600-608.

Muller J.P. *et al.* (1992) *Applied Geochemistry* **1**: 205-216.

Muller J.P. & Calas G. (1993) « Genetic significance of paramagnetic centers in kaolinites » in *Kaolin genesis and utilization*, H. H. Murray, W. Bundy and C.Harvey, eds., The Clay Minerals Society, Boulder, 341 p.

Muller J.P. & Calas G. (1993) *Geochimica et Cosmochimica Acta* **57**: 1029-1037.

Muller J.P. *et al.* (1995) *American Journal of Science* **295**: 115-155.

Murad E. & Wagner U. (1991) *Neues Jahrbuch Mineralogie Abhteilung* **162**: 281-309.

Nahon D.& Merino E. (1996) *Journal of Geochemical Exploration* **57**: 217-225.

Plançon A. *et al.* (1989) *Clays and Clay Minerals* **37**: 203-210.

Schroeder P.A. & Pruett R.J. (1996) *American Mineralogist* **81**: 26-38.

Sorieul S. *et al.* (2005) *Physics and Chemistry of Minerals* **32**: 1-7.

Tardy Y. (1993) *Pétrologie des latérites et des sols tropicaux*, Masson, Paris.

Tardy Y. & Roquin C. (1998) *Dérive des continents. Paléoclimats et altérations tropicales*. Editions BRGM, Orléans.

Théveniaut H. & Freyssinet Ph. (1999) *Palaeo* **148**: 209-231.

Volume 1: Bertrand P. (2020) *Electron Paramagnetic Resonance Spectroscopy - Fundamentals*, Springer, Heidelberg.

Wang D. & Hanson G.R. (1995) *Journal of Magnetic Resonance* A **117**: 1-8.